Satellite-observed sea surface salinity: real trends or instrumental drifts?

Author: Paula Plana Casadellà, pplanaca91@alumnes.ub.edu
Facultat de Física, Universitat de Barcelona, Diagonal 645, 08028 Barcelona, Spain.

Advisors: Estrella Olmedo Casal, Verónica González Gambau,
Aina García Espriu, Ferran Macià Bros (ferran.macia@ub.edu)

Abstract: Monitoring global water cycle intensification through satellite sea surface salinity (SSS) requires distinguishing genuine geophysical trends from instrumental artifacts. This work analyses eight years (2011–2018) of uncorrected SMOS observations to address this problem without relying on external reference datasets. By fitting independent linear regressions for each combination of geographic and antenna-frame coordinates, antenna-frame consistency (trend invariance across the instrument's field of view) is used as the primary diagnostic for signal separation. Trend significance is assessed via a Student's T test at the 95% confidence level. An exploratory classification of ocean cells within $\pm 60^{\circ}$ latitude identifies 52.7% as geophysical trends and 23.5% as instrumental artifacts, with the remainder being inconclusive or statistically non-significant. These results demonstrate that antenna-frame analysis recovers genuine geophysical variability that can be dismissed as noise or removed by standard bias correction and filtering procedures.
Keywords: Sea surface salinity (SSS), SMOS mission, geophysical trends, instrumental drifts, antenna-frame consistency, water cycle.
SDGs: This work is related to the sustainable-development goals (SDGs) 13 and 14.

I. INTRODUCTION

In the current scenario of global warming, it is hypothesized that the water cycle is intensifying, following the "Dry gets Drier and Wet gets Wetter" paradigm [1]. Traditionally, sea surface salinity (SSS) has been characterized as an ocean rain gauge reflecting the balance between evaporation and precipitation ($E - P$). However, recent research emphasizes that this is an oversimplification for long-term studies. SSS variability is not solely driven by local freshwater fluxes, but is also heavily influenced by internal ocean processes [2]. Despite this complexity, satellite-derived SSS has been found to capture the intensification of the water cycle more prominently than near surface salinity (NSS) measurements at depth provided by *in situ* sensors, which are often diluted by the ocean internal dynamics. This makes remote-sensed SSS a unique and essential tool for climate monitoring. It provides synoptic and global observations, overcoming the scarce and sparse sampling of traditional *in situ* NSS measurements [1].

Beyond these sampling differences, a key complication is that satellite and *in situ* instruments sample physically distinct ocean layers. *In situ* instruments typically monitor NSS at depths greater than 0.5 m, whereas satellite radiometers sensitive to salinity capture radiation originating from the uppermost ~ 1 cm of the ocean surface. Discrepancies between the two are therefore not always instrumental in origin; they can reflect real geophysical signals such as fresh lenses from rain or river plumes trapped at the surface [2], or increased stratification of the ocean upper layers induced by surface warming [1].

This research was carried out at the Barcelona Expert Centre (BEC), Institut de Ciències del Mar (ICM-CSIC), a joint initiative specialised in developing retrieval algorithms for the European Space Agency's (ESA) Soil Moisture and Ocean Salinity (SMOS) mission. Since 2009, SMOS has operated in a sun-synchronous orbit, providing continuous global observations of brightness temperature (T_{B}) through ascending and descending semiorbits [3]. The platform carries the Microwave Imaging Radiometer with Aperture Synthesis (MIRAS), a Y-shaped interferometric antenna operating at 1.41 GHz (L-band). Unlike other real aperture radiometers, its aperture synthesis enables the acquisition of a full T_{B} image every 2.4 s, allowing a given surface location to be observed multiple times from different incidence angles [4]. This multi-angular viewing capability provides the physical basis for discerning a common geophysical signal from antenna-dependent instrumental artifacts.

Salinity is measured according to the Practical Salinity Scale (PSS-78, following UNESCO guidelines), under which the values are unitless. Retrieving SSS from SMOS observations is technically demanding because the sensitivity of T_{B} to salinity is limited and the changes must be detected within the narrow variability of the open ocean (typically between 32 and 38). Moreover, L-band is affected by Radio Frequency Interferences (RFI) from man-made sources, which can induce artificial temporal variations of SSS even in areas far from land [2].

In this work, the trends observed in the SMOS SSS time series are decomposed into three primary components: true geophysical signals, which provide insight into the intensification of the water cycle; long-term instrumental drifts, arising from sensor aging; and RFI-induced artifacts. To isolate these components, a granular approach is implemented where measurements are evaluated according to their specific acquisition conditions: their coordinates within the antenna frame (ξ,η), their geographic location, and their orbital direction (ascending or descending). This strategy is necessary because instrumental errors have been shown to depend significantly on both the antenna position and the orbital direction [2, 3].

The foundation of this study lies in the preliminary work conducted by the candidate during an internship at the ICM-CSIC, dedicated to initial data handling and script development to calculate SSS trends. The current work expands these efforts into a rigorous analysis of an eight-year dataset (2011–2018), implementing statistical significance tests and focusing on the physical interpretation of the results. The primary objective is to provide an accurate estimate of geophysical SSS trends by isolating them from potential instrumental drifts and RFI without relying on external reference data, such as *in situ* measurements, which could introduce discrepancies due to their different observational nature. The study is based on the hypothesis that genuine geophysical signals exhibit consistency across the instrument's field of view, whereas instrumental artifacts manifest as antenna coordinate-dependent inconsistencies.

II. METHODOLOGY

A. Data and acquisition conditions

The dataset comprises eight years (2011–2018) of global, uncorrected SSS observations from the SMOS mission, totaling approximately 1 TB of data stored in NetCDF format (binary format with a non-negligible learning curve for new users). Each SSS measurement is associated with the following acquisition conditions:

1. *Orbital direction:* Whether the satellite semiorbit is ascending or descending.
2. *Antenna-frame position:* The position within the MIRAS field of view, defined by the antenna coordinates (ξ,η) and represented by a discrete index ranging from 0 to 2270.
3. *Geographic location:* The geographic position of the measurement, discretized into bins of 0.25° latitude-longitude spatial resolution.

Ascending and descending semiorbits are processed independently to account for their different patterns of instrumental drifts and RFI contamination [2, 3]. For each orbital direction, the *antenna-frame position* and the *geographic location* define the discrete bins used to organize the salinity observations over the eight-year period, with time as the independent variable for subsequent linear regression analysis. The results presented in this work correspond to ascending semiorbits only.

B. Mathematical framework

The slope ($\hat{\beta}$) and intercept ($\hat{\alpha}$) are estimated using a simple linear regression applied to the time series. They are calculated for each acquisition condition using the ordinary least squares (OLS) method, following the methodology used by Olmedo *et al.* [1]. They are obtained from five base statistics: the observation count (N), $\sum t_i$, $\sum x_i$, $\sum t_i^2$, and $\sum t_i x_i$, where x_i represents the SSS measurements (in PSS-78) and t_i denotes the time coordinates in days relative to the first date of the analyzed time series (January 5, 2011):

$$\hat{\beta} = \frac{N\sum_{i=1}^{N} t_i x_i - \sum_{i=1}^{N} t_i \sum_{i=1}^{N} x_i}{N\sum_{i=1}^{N} t_i^2 - \left(\sum_{i=1}^{N} t_i\right)^2}, \tag{1}$$

$$\hat{\alpha} = \frac{\sum_{i=1}^{N} x_i \sum_{i=1}^{N} t_i^2 - \sum_{i=1}^{N} t_i \sum_{i=1}^{N} t_i x_i}{N\sum_{i=1}^{N} t_i^2 - \left(\sum_{i=1}^{N} t_i\right)^2}. \tag{2}$$

To enable subsequent statistical validation without reprocessing the entire eight-year dataset, the sum of the squares of the SSS values ($\sum x_i^2$) is also accumulated alongside the five base statistics. This quantity allows the total variability of the salinity observations relative to their mean to be computed directly, using the identity:

$$\sum_{i=1}^{N}(x_i - \bar{x})^2 = \sum_{i=1}^{N} x_i^2 - N\bar{x}^2, \tag{3}$$

where $\bar{x}$ represents the arithmetic mean of the SSS values.

To ensure the statistical reliability of the estimated SSS trends, a Student's T test is applied to the resulting $\hat{\beta}$ for every acquisition condition. While this procedure follows the significance criteria used by Olmedo *et al.* [1], this work extends the application of the test to the antenna-frame level. The procedure tests the null hypothesis that no trend exists, with the t-statistic computed as:

$$t = \frac{|\hat{\beta}| \cdot \sqrt{\sum_{i=1}^{N}(t_i - \bar{t})^2}}{\sqrt{\frac{1}{N-2}\sum_{i=1}^{N}(x_i - \bar{x})^2}}, \tag{4}$$

where $\bar{x}$ and $\bar{t}$ represent the arithmetic means of the SSS and time coordinates, respectively. The factor $N-2$ represents the degrees of freedom for a linear regression with two estimated parameters ($\hat{\alpha}$ and $\hat{\beta}$). These means are computed using the pre-accumulated sums, allowing batch processing of the large dataset without needing to keep the full time series in memory. A trend is considered significant if it meets two specific requirements [1]:

1. *Observation count (N):* The total number of observations must satisfy $N > 100$ to ensure a sufficient statistical sample.

2. *Confidence level:* The calculated t-statistic must exceed the threshold for a 95% confidence level ($|t| > 1.65$ for $N > 100$).

However, the Student's T-test assumes independent observations, whereas SSS time series may exhibit serial correlation, which can lead to overestimated significance. Therefore, refining the assessment with bootstrap-based tests [5], for example, is a proposed future refinement.

C. Computational implementation

Processing the eight-year dataset constitutes the primary computational demand of this work. Given its high volume, the analysis was executed on the Drago High-Performance Computing (HPC) cluster using a modular Python pipeline developed with the `xarray` and `numpy` libraries. Designed for parallel execution, the pipeline processes data in monthly chunks and batches of 128 antenna indices. Intermediate accumulated sums are stored as NetCDF files to allow resumption in case of failure. Execution time was further optimised through full vectorization across all acquisition conditions.

To increase the number of observations available at each geographic cell, reducing noise caused by sparse sampling in specific regions of the ocean, a spatial integration step was implemented. Prior to estimating the regression parameters ($\hat{\beta}$, $\hat{\alpha}$), the six accumulated statistics of each geographic cell are updated by aggregating the contributions of its eight first neighbors:

$$V_{\text{filtered}}(\varphi, \lambda) = \sum_{\varphi'=\varphi-\Delta}^{\varphi+\Delta} \sum_{\lambda'=\lambda-\Delta}^{\lambda+\Delta} V(\varphi', \lambda'), \tag{5}$$

where φ and λ denote latitude and longitude, respectively, $\Delta = 0.25°$ is the bin resolution, and V represents any of the six accumulated statistics. The longitude axis applies periodic boundary conditions (wrap-around at $\pm 180°$). This spatial integration is justified by the assumption that geophysical variability at scales of 0.25° is small relative to the antenna-frame variability (an assumption that future work could revisit without raw-data reprocessing, given the modular pipeline design). No explicit land mask has been applied during this stage; coastal cells may therefore receive contributions from land-contaminated observations and their trend estimates should be interpreted with caution.

To optimise storage usage, a linear quantization strategy was implemented, achieving an initial 50% reduction in storage volume. Floating-point SSS values (S_{f}) are transformed into 64-bit integers (S_{q}) as follows:

$$S_{\text{q}} = \text{round}\left((S_{\text{f}} - \text{offset}) \cdot 10{,}000\right). \tag{6}$$

This approach maintains a physical precision of 10^{-4} (in PSS-78), several orders of magnitude smaller than the MIRAS radiometric noise [2], ensuring no loss of physical information. Combined with NetCDF compression, this strategy achieved an overall 75% reduction in the total storage footprint.

III. RESULTS AND DISCUSSION

Once the accumulated statistics have been computed for the full 2011–2018 period, the OLS regression yields a trend estimate $\hat{\beta}$ for every combination of geographic location and antenna coordinate. The dimensionality of $\hat{\beta}$ defines two complementary visualization strategies: projection onto the geographic plane (rendered using the `cartopy` library), collapsing the antenna axis through statistics such as the mean or standard deviation; and projection onto the antenna frame (ξ, η) for a fixed geographic location, revealing how the trend varies across the instrument's field of view. The study area is restricted to the $\pm 60°$ latitude range, as the datasets used lack the processing required for high-latitude regions.

A. Case studies in the antenna frame

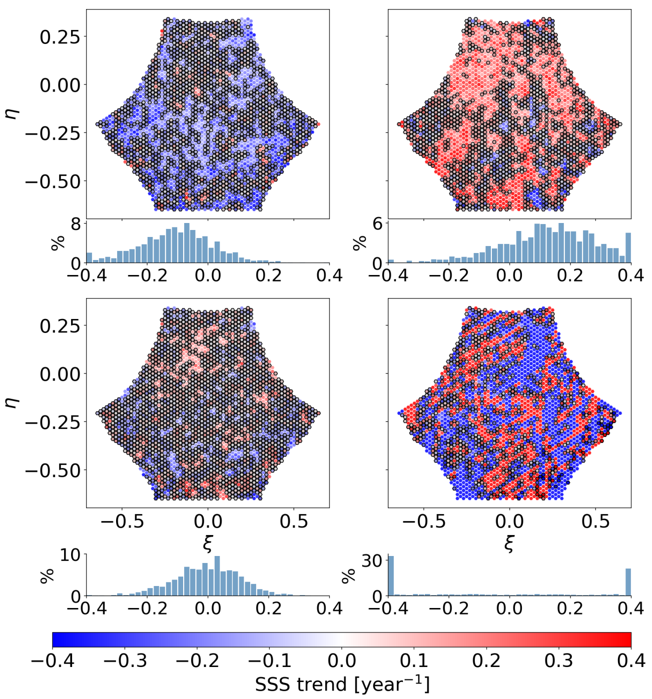

FIG. 1: Antenna-frame projection of the SSS trends [year^{-1}] for four fixed geographic regions. Black contours identify coordinates where trends are not statistically significant according to the Student's T test applied. *Top left:* Western Pacific Warm Pool (15°N, 160°W). *Top right:* southern Indian Ocean (20°S, 110°E). *Bottom left:* central tropical Pacific (5°S, 130°W). *Bottom right:* East China Sea (37°N, 145°E). The bins at the boundaries of a histogram accumulate all values falling outside the displayed range.

Figure 1 projects trend estimates onto the antenna frame (ξ, η) for four representative geographic regions. This projection illustrates the complexity of the retrieved signals and motivates the classification framework developed in the following section. The top left and top right figures display a high consistency across the instrument's field of view, showing a clear predominance of negative and positive trends, respectively, in agreement with the results found in Olmedo *et al.* (2022) [1]. The bottom left region exhibits a heterogeneous pattern, with positive and negative estimates intermixed across the antenna frame. A common feature across these regions is the prevalence of statistically non-significant estimates (black contours), which is physically expected given the uncorrected nature of the analysed data, the high uncertainty associated with uncorrected observations and the relatively short temporal baseline. The bottom right region stands out because, despite a substantial fraction of significant estimates, the trends are spatially incoherent within the antenna frame; a signature that points to an instrumental rather than geophysical origin.

B. Global trend maps and statistical classification

Figure 2 summarises the eight-year SSS evolution through four complementary geographic projections. The mean trend map (top left) reveals large-scale structures consistent with known oceanographic regimes, such as the trends in the tropical Pacific and the southern Indian Ocean. However, several regions exhibit extreme, anomalous trends that are unlikely to be geophysical. Specifically, the North Atlantic, the Gulf of Alaska, and the East China Sea, appear as spatially anomalous structures that differ from the smooth spatial patterns of the geophysical signals, and are characteristic of Radio Frequency Interferences (RFI) contamination [2]. It is worth noting that this analysis of uncorrected SSS data reveals a wider range of trends than the ± 0.05 year^{-1} interval identified by Olmedo *et al.* (2022) [1], showing the added value of computing trends with minimum data processing of the observations.

The standard deviation (σ) of the trends across all antenna coordinates is shown in the top right panel in Figure 2. While geophysical signals are expected to be antenna-coordinate invariant (yielding a low σ), instrumental artifacts are coordinate-dependent and manifest as regions of high dispersion. The distribution peaks at $\sigma \sim 0.25$ year^{-1}, which is adopted here as an exploratory empirical threshold to distinguish low from high dispersion. Determining a statistically optimal boundary is deferred to future work. Regions of high σ coincide with the most saturated and anomalous regions identified in the top left plot in Figure 2. This correlation reinforces their non-geophysical interpretation, suggesting an origin associated with RFI or other coordinate-dependent instrumental effects.

The percentage of statistically significant antenna coordinates (S) for a given ocean cell (bottom left map) exhibits a distribution peaking at approximately $S = 10\%$. This highlights how critical salinity trend estimation is and the substantial impact that different acquisition-related error sources have, even in regions where RFI is not expected to be present. This value is adopted as the empirical threshold below which cells are classified as statistically non-significant.

The sign dominance map (bottom right) quantifies the agreement in trend sign among statistically significant antenna coordinates. It is defined here as $D = f_+ - 50\%$, where f_+ is the percentage of positive trends, such that $D = 0$ corresponds to equal sign balance and $|D| > 5\%$ indicates a sign agreement exceeding 55%. The distribution peaks near zero, reflecting widespread sign heterogeneity across the antenna frame. Consequently, ocean cells with $|D| < 5\%$ are masked as inconclusive (gray overlay). This threshold, identified where the distribution flattens, represents a conservative choice that errs toward excluding inconclusive cells; future work should explore more robust criteria. Building on the antenna-coordinate invariance requirement established above, statistically significant trends are classified as follows:

1. *Geophysical trend:* Regions where more than 10% of antenna coordinates yield a significant trend ($S > 10\%$), exhibit low standard deviation (relative to the peak of the distribution, $\sigma \leq 0.25$ year^{-1}), and show consistent sign agreement ($D > 5\%$).

2. *Instrumental artifact (RFI or bias):* Regions where more than 10% of antenna coordinates yield a significant trend ($S > 10\%$) and show high standard deviation ($\sigma > 0.25$ year^{-1}, corresponding to the onset of the distribution tail). Sign dominance is not a classifying criterion here, as these contaminated regions may exhibit either strong or weak sign agreement.

The bottom right panel in Figure 2 represents this classification by marking regions classified as instrumental artifacts in yellow. Applying the classification scheme globally, 52.7% of valid ocean cells within $\pm 60°$ latitude are classified as geophysical, 23.5% as instrumental artifacts, 16.6% show insufficient sign agreement to establish a consistent trend direction, and 7.2% lack sufficient statistical significance for any classification.

IV. CONCLUSIONS

This exploratory study provides evidence that antenna-frame consistency is an effective diagnostic for separating geophysical SSS trends from instrumental artifacts in uncorrected SMOS data, without relying on external reference datasets. Our exploratory classification reveals that 52.7% of valid ocean cells within $\pm 60°$

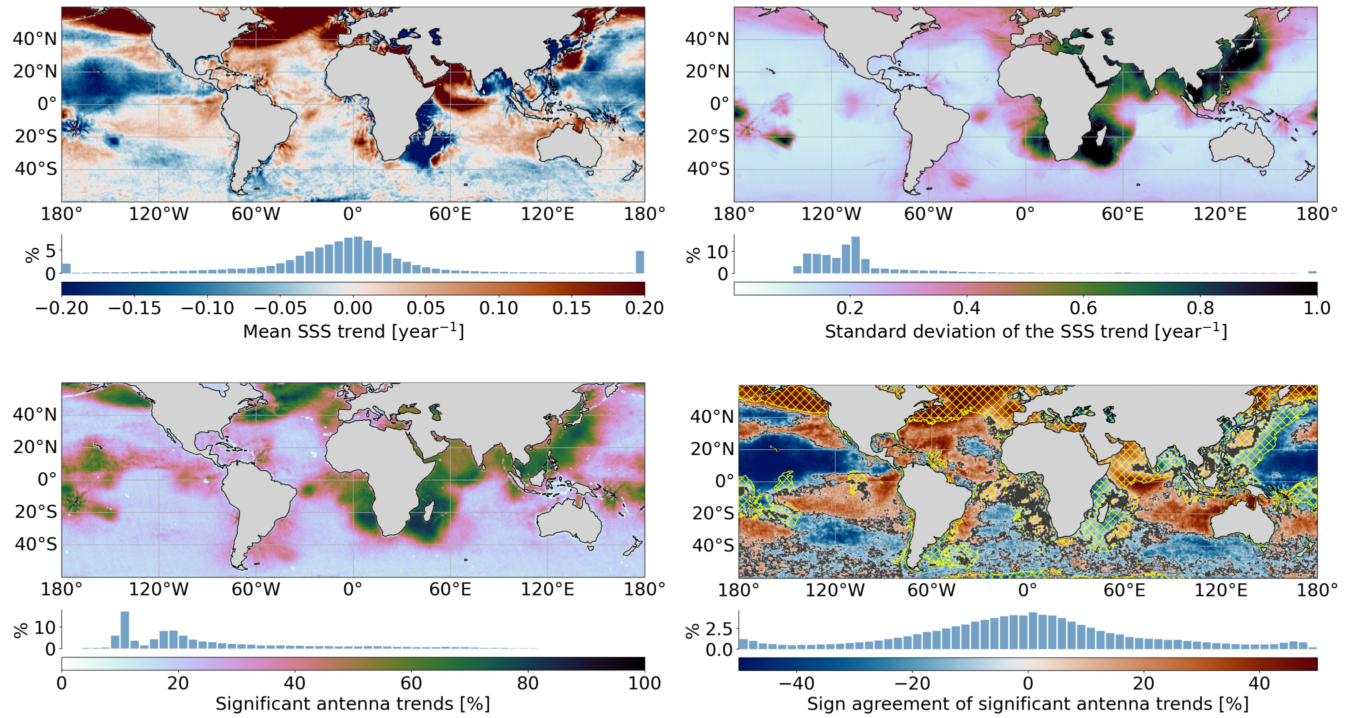

FIG. 2: Geographic projections of the SSS trend analysis. *Top left:* mean trend across all antenna coordinates [year^{-1}]. *Top right:* antenna-frame standard deviation (σ) [year^{-1}]. *Bottom left:* percentage of antenna coordinates yielding a statistically significant trend at the 95% confidence level. *Bottom right:* sign dominance among significant coordinates; yellow overlay marks regions with $\sigma > 0.25$ year^{-1}; gray overlay marks regions where $|D| < 5\%$.

latitude exhibit geophysical trends. In contrast, 23.5% are dominated by instrumental artifacts, concentrated in RFI-prone areas like the North Atlantic and the East China Sea, while the remaining 23.8% stay inconclusive due to insufficient sign dominance or lack statistical significance.

These results have direct implications for the development of SSS retrieval algorithms: incorporating antenna-frame consistency can prevent the inadvertent removal of genuine geophysical variability during bias correction and filtering procedures. As this is an initial assessment, future work should extend the analysis to descending semiorbits, apply RFI mitigation prior to the trend estimation, and validate findings against independent satellite products, ocean models, and *in situ* data.

Acknowledgments

I acknowledge the use of the Drago HPC cluster for data processing and of AI-assisted tools to improve the wording. Source code available at: `https://github.com/paulaplana/SMOS_SSS_trends`. I thank my advisors Estrella, Verónica, and Aina for greatly enriching my stay at the ICM, together with Joan and Arnau. I am also grateful to my loved ones, especially my friends Alba, Dani, Sara and Maria, and my partner Jordi.

---

[1] Olmedo, E. et al.. "Increasing stratification as observed by satellite sea surface salinity measurements". Sci. Rep. **12**: 6279 (2022).

[2] Reul, N. et al.. "Sea surface salinity estimates from spaceborne L-band radiometers: An overview of the first decade of observation (2010-2019)". Remote Sens. Environ. **242**: 111769 (2020).

[3] Oliva, R. et al.. "SMOS Third Mission Reprocessing after 10 Years in Orbit". Remote Sens. **12**: 1645 (2020).

[4] Martín-Neira, M. et al.. "SMOS instrument performance and calibration after six years in orbit". Remote Sens. Environ. **180**: 19-39 (2016).

[5] Noguchi, K. et al.. "Bootstrap-based tests for trends in hydrological time series, with application to ice phenology data". J. Hydrol. **410**: 150-161 (2011).

Salinitat superficial del mar observada per satèl·lit: tendències reals o derives instrumentals?

Author: Paula Plana Casadellà, pplanaca91@alumnes.ub.edu
Facultat de Física, Universitat de Barcelona, Diagonal 645, 08028 Barcelona, Spain.

Advisors: Estrella Olmedo Casal, Verónica González Gambau,
Aina García Espriu, Ferran Macià Bros (ferran.macia@ub.edu)

Resum: El monitoratge de la intensificació del cicle global de l'aigua mitjançant la salinitat superficial del mar (SSS) observada per satèl·lit requereix distingir les tendències geofísiques reals dels artefactes instrumentals. Aquest treball analitza vuit anys (2011–2018) d'observacions SMOS sense corregir per abordar aquest problema sense recórrer a conjunts de dades de referència externs. Mitjançant l'ajust de regressions lineals independents per a cada combinació de coordenades geogràfiques i coordenades del marc de l'antena, la consistència en el marc de l'antena (invariància de les tendències al llarg del camp de visió de l'instrument) s'utilitza com a criteri diagnòstic principal per a la separació dels senyals. La significació de les tendències s'avalua mitjançant una prova t de Student al nivell de confiança del 95%. Una classificació exploratòria de les cel·les oceàniques dins del rang de $\pm 60^\circ$ de latitud identifica el 52,7% com a tendències geofísiques i el 23,5% com a artefactes instrumentals, mentre que la resta són inconcluses o estadísticament no significatives. Aquests resultats demostren que l'anàlisi en el marc de l'antena permet recuperar variabilitat geofísica real que pot ser descartada com a soroll o eliminada pels procediments estàndard de correcció de biaixos i filtratge.
Paraules clau: salinitat superficial del mar (SSS), missió SMOS, tendències geofísiques, derives instrumentals, consistència en el marc de l'antena, cicle de l'aigua.
ODSs: Aquest treball està relacionat amb els Objectius de Desenvolupament Sostenible (ODS) 13 i 14.

Objectius de Desenvolupament Sostenible (ODSs o SDGs)

1. Fi de la es desigualtats		10. Reducció de les desigualtats	
2. Fam zero		11. Ciutats i comunitats sostenibles	
3. Salut i benestar		12. Consum i producció responsables	
4. Educació de qualitat		13. Acció climàtica	X
5. Igualtat de gènere		14. Vida submarina	X
6. Aigua neta i sanejament		15. Vida terrestre	
7. Energia neta i sostenible		16. Pau, justícia i institucions sòlides	
8. Treball digne i creixement econòmic		17. Aliança pels objectius	
9. Indústria, innovació, infraestructures			

El contingut d'aquest TFG, part d'un grau universitari de Física, es relaciona amb l'ODS 13, i en particular amb la fita 13.3 per la seva contribució al monitoratge i la comprensió de la intensificació del cicle de l'aigua en un context de canvi climàtic. També es pot relacionar amb l'ODS 14, fita 14.A, per l'avenç en el coneixement científic de la salut dels oceans mitjançant l'anàlisi de la salinitat superficial.